H_2O-Based Solid Fuel Power Source Based on the Catalysis of H by HOH Catalyst

R. Mills[1], J. Lotoski

BlackLight Power, Inc., 493 Old Trenton Road, Cranbury, NJ 08512, USA

Abstract: Atomic hydrogen is predicted to form fractional Rydberg energy states $H(1/p)$ called "hydrino atoms" wherein $n = \frac{1}{2}, \frac{1}{3}, \frac{1}{4}, ..., \frac{1}{p}$ ($p \leq 137$ is an integer) replaces the well-known parameter $n = \text{integer}$ in the Rydberg equation for hydrogen excited states. The transition of H to a stable hydrino state $H\left[\frac{a_H}{p = m+1}\right]$ having a binding energy of $p^2 \cdot 13.6\ eV$ occurs by a nonradiative resonance energy transfer of $m \cdot 27.2\ eV$ (m is an integer) to a matched energy acceptor such as nascent H_2O that has a potential energy of 81.6 eV (m = 3). The energy transfer to the HOH catalyst results in its ionization wherein the charge build up may become limiting of the further propagation of the catalysis reaction. An applied, low-voltage, high current was predicted to ameliorate this space charge inhibition of the hydrino reaction. To achieve these conditions, a solid fuel was used that comprises a highly conductive matrix such as a metal powder with bound or suspended H_2O that served as the source of HOH catalyst and H. When the high current was applied, the H_2O-based solid exploded with a tremendous burst of optical power as recorded with high-speed video and spectroscopically. The power density was confirmed to be about 3 X 10^{10} W/liter of fuel volume using the measured time of the event and the energy released as measured by bomb calorimetry. The predicted molecular hydrino $H_2(1/4)$ was identified as a product by Raman spectroscopy, photoluminescence emission spectroscopy, and X-ray photoelectron spectroscopy (XPS).

Key Words: new energy source, HOH catalysis, hydrinos, H_2O-based solid fuel, high kinetics

[1] Corresponding author: 609-490-1090 (phone); 609-490-1066 (fax); rmills@blacklightpower.com

I. Introduction

Classical physical laws predict that atomic hydrogen may undergo a catalytic reaction with certain species, including itself, that can accept energy in integer multiples of the potential energy of atomic hydrogen, $m \cdot 27.2$ eV, wherein m is an integer. The predicted reaction involves a resonant, nonradiative energy transfer from otherwise stable atomic hydrogen to the catalyst capable of accepting the energy. The product is H(1/p), fractional Rydberg states of atomic hydrogen called "hydrino atoms," wherein n = 1/2, 1/3, 1/4,…, 1/p ($p \leq 137$ is an integer) replaces the well-known parameter n = integer in the Rydberg equation for hydrogen excited states. Each hydrino state also comprises an electron, a proton, and a photon, but the field contribution from the photon increases the binding energy rather than decreasing it corresponding to energy desorption rather than absorption. Since the potential energy of atomic hydrogen is 27.2 eV, m H atoms serve as a catalyst of $m \cdot 27.2\ eV$ for another $(m+1)$th H atom [1]. For example, a H atom can act as a catalyst for another H by accepting 27.2 eV from it via through-space energy transfer such as by magnetic or induced electric dipole-dipole coupling to form an intermediate that decays with the emission of continuum bands with short wavelength cutoffs and energies of $m^2 \cdot 13.6\ eV$ $\left(\frac{91.2}{m^2}\ nm\right)$. In the H-atom catalyst reaction involving a transition to the $H\left[\frac{a_H}{p=m+1}\right]$ state, m H atoms serve as a catalyst of $m \cdot 27.2\ eV$ for another $(m+1)$th H atom. Then, the reaction between $m+1$ hydrogen atoms whereby m atoms resonantly and nonradiatively accept $m \cdot 27.2\ eV$ from the $(m+1)$th hydrogen atom such that mH serves as the catalyst is given by

$$m \cdot 27.2\ eV + mH + H \rightarrow mH^+_{fast} + me^- + H*\left[\frac{a_H}{m+1}\right] + m \cdot 27.2\ eV \quad (1)$$

$$H*\left[\frac{a_H}{m+1}\right] \rightarrow H\left[\frac{a_H}{m+1}\right] + [(m+1)^2 - 1^2] \cdot 13.6\ eV - m \cdot 27.2\ eV \quad (2)$$

$$mH^+_{fast} + me^- \rightarrow mH + m \cdot 27.2\ eV \quad (3)$$

And, the overall reaction is

$$H \rightarrow H\left[\frac{a_H}{p=m+1}\right] + [(m+1)^2 - 1^2] \cdot 13.6\ eV \quad (4)$$

In addition to atomic H, a molecule that accepts $m \cdot 27.2\ eV$ from atomic H with a decrease in the magnitude of the potential energy of the molecule by the same energy may also serve as a catalyst. The potential energy of H_2O is 81.6 eV [1]; so, the nascent H_2O molecule (not hydrogen bonded in solid, liquid, or gaseous state) may serve as a catalyst. Based on the 10% energy change in the heat of vaporization in going from ice at 0°C to water at 100°C, the

average number of H bonds per water molecule in boiling water is 3.6 [1]; thus, H_2O must be formed chemically as isolated molecules with suitable activation energy in order to serve as a catalyst to form hydrinos. The catalysis reaction $\left(m=3\right)$ regarding the potential energy of nascent H_2O is

$$81.6\ eV + H_2O + H\left[a_H\right] \rightarrow 2H^+_{fast} + O^- + e^- + H*\left[\frac{a_H}{4}\right] + 81.6\ eV \tag{5}$$

$$H*\left[\frac{a_H}{4}\right] \rightarrow H\left[\frac{a_H}{4}\right] + 122.4\ eV \tag{6}$$

$$2H^+_{fast} + O^- + e^- \rightarrow H_2O + 81.6\ eV \tag{7}$$

And, the overall reaction is

$$H\left[a_H\right] \rightarrow H\left[\frac{a_H}{4}\right] + 81.6\ eV + 122.4\ eV \tag{8}$$

An electrochemical CIHT (Catalyst Induced Hydrino Transition) cell generates electricity from H_2O vapor that may be extracted from air using a charge and discharge cycle to convert the H_2O into hydrinos, oxygen, and excess electricity. During a charging phase, hydrogen and oxygen are generated by electrolysis of H_2O at the anode and cathode, respectively. Then, the cell is discharged and electrolytic OH^- is oxidized at the anode, OH^- reacts with H to form HOH, and hydrinos are formed from the catalysis of H by HOH catalyst. The electrochemical cell reactions consume initially the hydrogen and then H_2O fed to the cell to produce a large gain in electrical output. The CIHT electrical energies were continuously output over long-duration, measured on different systems, configurations, and modes of operation and were typically multiples of the electrical input that in recent higher-power-density cases exceed the input by a factor of about 2 at about 10 mW/cm^2 anode area. The power density was further increased by a factor of over 10 while maintaining gain by running a corresponding high current [2-4].

Thermal energy may also be produced from the catalysis of H to H(1/4) wherein nascent H_2O serves as the catalyst, and a chemical reaction is the source of atomic hydrogen and catalyst. Solid fuels that form HOH catalyst and H also showed multiple times the maximum theoretical energy [5]. Excess heats from solid fuels reactions were measured using water-flow calorimetry and these results have been independently confirmed by differential scanning calorimetry (DSC) runs at testing laboratories. The predicted molecular hydrino $H_2(1/4)$ was identified as a product of power producing cells, CIHT cells and thermal cells, by techniques such as MAS ^1H NMR, ToF-SIMS, ESI-ToFMS, electron-beam excitation emission spectroscopy, Raman spectroscopy, Raman spectroscopy with surface enhanced Raman scattering (SERS), time-of-flight secondary ion mass spectroscopy (ToF-SIMS), electrospray ionization time-of-flight mass spectroscopy (ESI-ToFMS), Fourier transform infrared (FTIR) spectroscopy, X-ray photoelectron XPS

spectroscopy, and photoluminescence emission spectroscopy [2-5]. Moreover, $m\,H$ catalyst was identified to be active in astronomical sources such as the Sun, stars, and interstellar medium wherein the characteristics of hydrino products match those of the dark matter of the universe [6-11].

Greater than 50 eV Balmer α line broadening that reveals a population of extraordinarily high-kinetic-energy hydrogen atoms in certain mixed hydrogen plasmas such as water vapor and continuum-emitting hydrogen pinch plasmas is a well-established phenomenon; however, the mechanism has been controversial in that the conventional view that it is due to field acceleration is not supported by the data and critical tests [12-24]. Rather it is shown that the cause is due to the energy released in the formation of hydrinos [25-31]. EUV radiation in the 10-30 nm region observed only arising from very low energy pulsed pinch gas discharges comprising some hydrogen first at BlackLight Power, Inc. (BLP) and reproduced at the Harvard Center for Astrophysics (CfA) [6-11] was determined to be due to the transition of H to the lower-energy hydrogen or hydrino state H(1/4) whose emission matches that observed wherein alternative sources were eliminated. HOH was identified as the most likely cause for the transition [6]. The high multiple kilo-amp current of the pinch plasma was a unique feature of this bright source of hydrino transition radiation.

Based on the catalyst mechanism, the high current facilitates a rapid transition rate (higher kinetics) by providing a sink for the inhibiting space charge build up from the ionization of the HOH catalyst. A Solid Fuel-Catalyst-Induced-Hydrino-Transition (SF-CIHT) cell disclosed previously [4] produces extraordinary power by using a solid fuel comprising a conductive matrix that has bound water. By confining the fuel between opposing electrodes of the cell, and applying a current of 12,000 A through the fuel, water ignites into an extraordinary brilliant flash of optical power released by the transition of hydrogen of H_2O into hydrinos. Specifically, it was shown previously that the kinetics of catalysis of H to H(1/4) by HOH catalyst can be explosive when a high current such as 10,000-20,000 A is flowed through the solid fuel [4] comprising M + H_2O (M = Ti, Cu, Al) that is a source of HOH catalysts and H. The resulting power density is about 1 X 10^{10} times greater than observed for the forerunner CIHT cell or thermal solid fuels [2-5]. The energy was attributed to the reaction of H_2O to $H_2(1/4)$ and $1/2O_2$. The transition of H to H(1/4) was confirmed by extreme ultraviolet (EUV) spectroscopy [6]. The HOH catalyst was shown to give EUV radiation in the region of less than 15 to 30 nm by igniting a solid fuel source comprising a source of H and HOH catalyst by passing a low-voltage, high current through the fuel to produce explosive plasma [6]. No chemical reaction can release such high-energy light, and the field corresponded to a voltage that was less than 15 V for the initially super-atmospheric collisional plasma. No high field existed

to form highly ionized ions that could give radiation in this region. This plasma source serves as strong evidence for the existence of the transition of H to hydrino H(1/4) by HOH as the catalyst.

In this paper, we test solid fuels of the SF-CIHT cell comprising bound H_2O for production of explosive power and excess energy. Specifically, the H_2O-based solid fuel such as one comprising Ti + H_2O was caused to explode by flowing a high current. The brilliant light-emitting plasma and its temporal evolution were characterized by high speed (6500 frames/s video) and a fast photodiode, respectively. The energy balance and time of the event were separately determined by bomb calorimetry and by the mechanical disruption time of the voltage and current waveform by the blast event and supporting the fast-response photodiode results, respectively. From these parameters and the fuel volume, the power and power density were determined. The predicted hydrino product $H_2(1/4)$ was identified by Raman spectroscopy, photoluminescence emission spectroscopy, and X-ray photoelectron spectroscopy (XPS).

II. Experimental

Calorimetry of Solid Fuel of the SF-CIHT Cell. The energy balances were measured on the H_2O-based solid fuels shown in Table 1 comprising M + H_2O or M + MO + H_2O (M = Ti, Cu, Al), Ag + $MgCl_2 \cdot 6H_2O$, Ti + $MgCl_2 \cdot 6H_2O$, Ti + $ZnCl_2$ + H_2O, Ag + NH_4NO_3 + H_2O, NH_4NO_3 + H_2O + Al, and NH_4NO_3. Hydrocarbon -based solid fuels comprised paraffin wax, Nujol oil, and synthetic oil 0W40. Metal foils heated in an argon-atmosphere glove box to dehydrate the hydrated surface oxide coat served as the calibration controls to determine the calorimeter heat capacity. An exemplary fuel comprised Cu (45 mg, Alfa Aesar stock# 41205, copper powder, 625 mesh, APS 0.50-1.5 micron, 99% (metals basis)) + CuO (45 mg, Alfa Aesar stock# 33307) + H_2O (30 mg) that was sealed in an aluminum DSC pan (75 mg) (aluminum crucible 30 µl, D: 6.7 mm X 3 mm (Setaram, S08/HBB37408) and aluminum cover D: 6.7 mm, stamped, tight (Setaram, S08/HBB37409)). Samples also comprised metal powder mixtures not contained in a DSC pan. The setup of the Parr 1341 calorimeter used for the energy balance determination (Figure 1) comprised an unmodified calorimeter jacket (21) and calorimeter cover (1) (combined Parr part number A1100DD). A thermistor with a temperature resolution of $\pm 0.0001^oC$ (2) (Parr part number 1168E2) passed through the calorimeter cover and was secured such that it read the water temperature in line with the bomb assembly at a distance of 2.54 cm from the bottom of the water bucket (19). The custom made, 0.051 cm thick stainless steel oval bucket weighed 417.8g and had a small diameter of 12.7 cm inches, a large diameter of 18.4 cm, and a height of 10.2 cm. The water bucket held 1225±.01 g of deionized water along with the custom calorimeter bomb assembly. A stirring assembly (6) comprised a stirrer pulley (Parr part number 37C2), a stirrer bearing assembly (Parr part number A27A), and stirrer shaft with impeller (11) (Parr part number A30A3). It was mounted on the calorimeter cover and was

connected to the motor assembly (Parr part number A50MEB) by a motor pulley (8) (Parr part number 36M4) by a stirrer drive belt (7) (Parr part number 37M2) driven by the motor (9). The motor assembly was attached to the calorimeter externally by an L-bracket motor connector (10) to prevent the heat output of the motor from affecting the calorimetric measurements. Two 1.6 cm OD solid copper electrodes (3) passed through customized holes in the calorimeter cover and further passed through a Teflon position stabilizing block and then connected to the main conductors of an ACME 75 kVA resistance welder. The 0.32 cm thick stainless steel custom cylindrical bomb cell (14) had a 7.62 cm diameter and 2.54 cm height with a 12.4 cm flange that was 0.64 cm thick. The electrodes penetrated the flange lid through electrode feed-throughs (13) with Teflon insulating ferrule seals (15) that provided electrical isolation and a hermetic seal. Power was transmitted to the solid fuel (18) through the 1.3 cm diameter 0.48 cm thick copper fastener swivel (17) by the 3.0 cm long, 0.95 cm diameter copper sample-fastening bolts (16) which were threaded through the base of the electrodes. The solid fuel was contained between the fastener swivels by tightening the sample fastening bolts to a torque of approximately 1.81 Nm as measured by a high accuracy flat beam torque wrench resulting in approximately 1112 N force to the sample as measured by a piezoresistive force sensor (Measurement Specialties, FC2311-0000-0250-L). Efficient heat transfer was enabled by heat fins (12) installed on the electrodes immediately above the electrode feed-throughs that ensured minimal heat loss through the electrodes and out of the closed system. The bucket stand (20) elevated the bomb cell to the top of the calorimeter to minimize the dimensions and quantities of materials necessary to operate the Parr 1341 calorimeter and improve the accuracy of the measurements.

Each sample was ignited under argon with an applied peak 60 Hz voltage of less than 10 V and a peak current of about 20,000 A. The input power was recorded through a custom interface receiving input from the positive probe connector (4) and negative probe connector (5). The input energy of the calibration and ignition of the solid fuel was given as the product of the voltage and current integrated over the time of the input. The voltage was measured by a data acquisition system (DAS) comprising a PC with a National Instruments USB-6210 data acquisition module and Labview VI. The current was also measured by the same DAS using a Rogowski coil (Model CWT600LF with a 700 mm cable) that was accurate to 0.3% as the signal source. V and I input data were obtained at 83 KS/s and a voltage attenuator was used to bring analog input voltage to within the +/-10V range of the USB-6210.

The input power data was processed to calculate the input energy during the rapid power decay following ignition to an open circuit. Taking the product of the measured voltage waveform obtained from the voltage taps immediately above the water level on the 5/8” OD Cu rods and the measured current waveform given by the Rogowski coil yielded the power waveform. The time integrated power waveform yielded the cumulative energy provided to the

system to the time point that the ignition or detonation event occurred. The secondary circuit of the spot welder transformer was temporarily broken as the electrode tips were pushed apart by the force of the blast. On a time scale of about 10 μs, the circuit quickly transitioned to high resistance, effectively becoming an open circuit with the development of a reactive voltage transient as a result of the fast collapsing magnetic flux in the transformer. The current fell to zero as the voltage transient produced a corresponding reflected wave reactive power component in the power waveform that typically rapidly decayed on the order of about 500 μs to 1 ms. To eliminate this reactive power component over the time of the current decay, the power waveform was smoothed over the immediate post-blast period until current reached zero by fitting the voltage and current components during this time to their typical amplitudes and phases during pre-blast conditions. The accuracy of this method was confirmed by the achievement of energy balance with control samples.

Figure 1. The setup of the Parr 1341 calorimeter used for the energy balance determination.

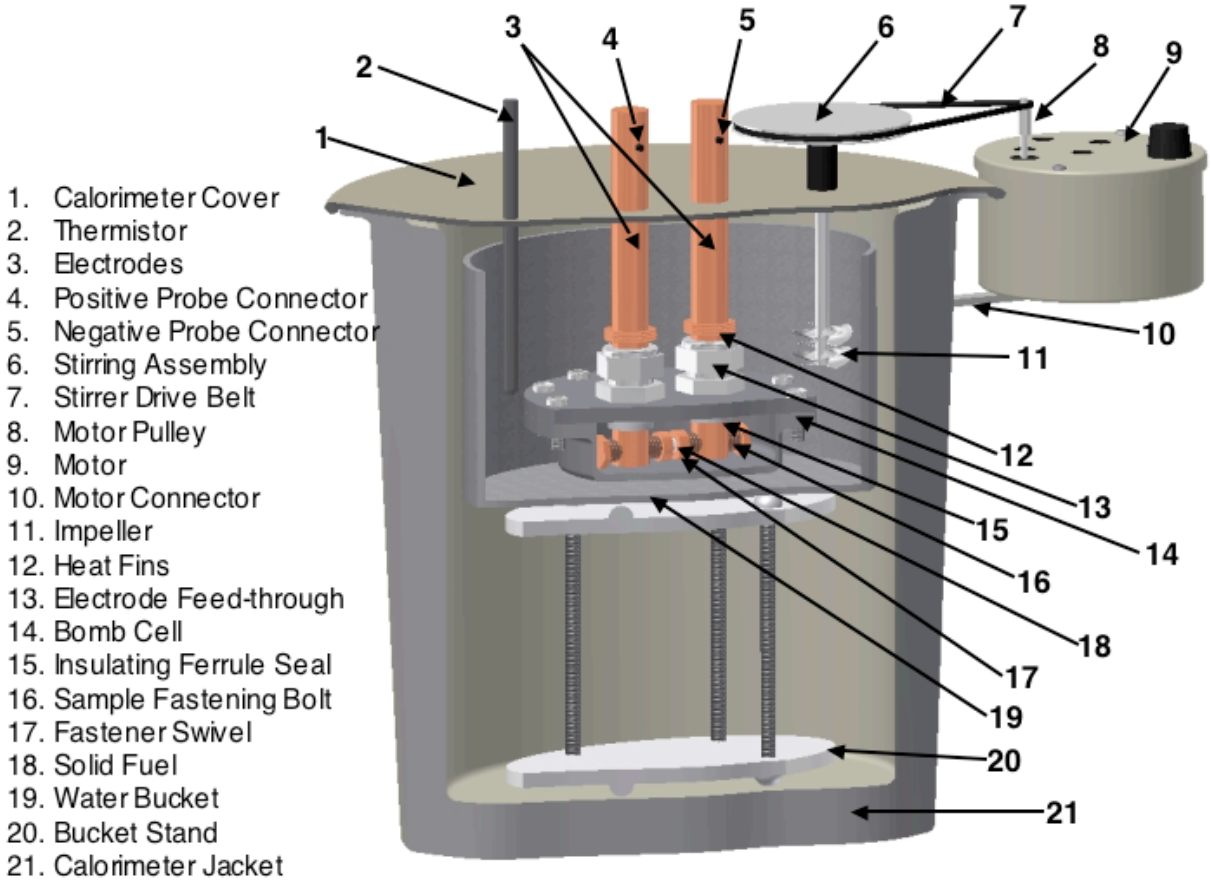

Ignition of H_2O-Based Solid Fuels with a Low Voltage, High Current and Plasma Duration Determination. Test samples comprising: (i) H_2O-based solid fuels 100 mg Cu[2] + 30 mg H_2O sealed in the DSC pan, and 100 mg Ti (Alfa Aesar stock# 10386, titanium powder, 325 mesh, 99% (metals basis) (< 44 micron)) + 30 mg H_2O sealed in the DSC pan, (ii) hydrocarbon-based solid fuel such as oil or paraffin wax sealed in the DSC pan, (iii) control H_2O-based reaction mixtures 185 mg In + 30 mg $CaCl_2$ + 15 mg H_2O, 185 mg In + 30 mg $ZnCl_2$ + 15 mg H_2O, 185 mg Bi + 30 mg $ZnCl_2$ + 5 mg H_2O, and 185 mg Sn + 30 mg $ZnCl_2$ + 5 mg H_2O, that were not catalytic to form hydrinos, and (iv) control conductive materials not comprising H_2O such as a 0.0254 cm diameter gold wire loop and a 2.38 mm diameter InSn wire loop, each oriented for axial current flow and preheated in vacuum/pre-dehydrated metal foils were loaded into the electrodes of the Acme 75 KVA welder that was activated to apply high current through each sample. The AC current was typically in the range of 10,000-30,000 A, and the peak voltage was typically less than 6 V with the exception of the wire samples having much lower current due to the low voltage and relatively high resistance. The expanding plasmas formed from solid fuel ignitions were recorded with a Phantom v7.3 high-speed video camera at 6500 frames per second.

The temporal evolution of the solid fuel Cu + H_2O sealed in the DSC pan was measured with a photodiode (Thorlabs, model SM05PD1A) having a spectral range of 350-1100 nm, a peak sensitive wavelength of 980 nm, an active area of 13 mm^2, a rise/fall time of 10 ns, and a junction capacitance of 24 pF at 20 V. The signal was processed using an amplifier (Opto Diode model PA 100) with no gain and a 10 V bias and recorded with a 60 MHz scope (Pico Technology, Picoscope 5442B) at a scan interval of 25 ns. The measuring distance was 25 cm. The temporal resolution of the photodiode was confirmed to be within specification by recording the response to a light-emitting diode powered by pulses of 1 μs, 10 μs, and 1 ms that were generated by a function generator (Agilent 33220A 20 MHz Arbitrary Waveform Generator). In each case, a square wave of the width of the temporal width of the pulse was observed.

Analytical Samples for the Spectroscopic Identification of Molecular Hydrino. The solid fuels that were used for calorimetric determination of the energy balance also served as sources of the theoretically predicted molecular hydrino product $H_2(1/4)$. The molecular hydrino samples comprised an indium witness plate or a KOH-KCl mixture placed in a sealed container under argon wherein hydrinos generated with ignition were trapped in the matrix of the indium or KOH-KCl mixture that thereby served as a molecular hydrino getter. Raman spectroscopy, photoluminescence emission spectroscopy, and X-ray photoelectron spectroscopy (XPS) were

[2] All metal samples comprised powder. H_2O was deionzed.

performed on reaction products. Starting materials not exposed to a hydrino source served as controls.

Quantitative X-ray diffraction (XRD). XRD was performed on the starting materials and the reaction products using a Panalytical X'Pert MPD diffractometer using Cu radiation at 45KV/40mA over the range 10° – 80° with a step size of 0.0131° and a counting time of 250 seconds per step. Once the patterns had been obtained, the phases were identified with the aid of the ICDD database and quantified by a Rietveld refinement.

Raman Spectroscopy. Raman spectroscopy was performed on indium metal foil witness plates and on solid 1g KCl + 1g KOH samples wherein each was held in a 1.45 cm OD X 2.5 cm height, open top Al_2O_3 crucible. The indium foil was exposed for one minute to the product gas following each ignition of a series of solid fuel pellet ignitions. Fifty solid fuel pellets were ignited sequentially in an argon atmosphere each comprising 100 mg Cu + 30 mg H_2O sealed in the DSC pan. Each ignition of the solid fuel pellet was performed using an Acme model 3-42-75 AR spot welder that supplied a short burst of electrical energy in the form of a 60 Hz low-voltage of about 8 V RMS and high-current of about 15,000 to 25,000 A. Spectra were obtained using a Thermo Scientific DXR SmartRaman spectrometer having a 780 nm diode laser. The resolution, depending on the instrument focal length, wavelength range, and grating, was typically 1-5 cm^{-1}. The Raman spectrum was also recorded on the In metal foil exposed to the product gas from the argon-atmosphere ignition of 50 mg of NH_4NO_3 sealed in the DSC pan.

The hydrino getter 1g KCl + 1g KOH was heated at 250 °C for 15 minutes and cooled (control), then placed in the crucible and exposed to 50 sequential ignitions of solid fuel pellets in an argon atmosphere at room temperature. Each pellet comprised 100 mg Cu + 30 mg H_2O sealed in the DSC pan. Additional solid fuels 80 mg Ti + 30 mg H_2O and 100 mg Ti + 50 mg Al + 30 mg $ZnCl_2$ + 15 mg H_2O were tested as powders with three ignition exposures each exposed to the hydrino getter KOH:KCl (1:1 wt%) that was not heated and was held in a stainless steel mesh pouch (32 X 32 per cm^2, 0.014 cm diameter wire). Each ignition of the solid fuel pellet was performed using a Acme model 3-42-75 AR spot welder that supplied a short burst of electrical energy in the form of a 60 Hz low-voltage of about 8 V RMS and high-current of about 15,000 to 25,000 A. The Raman spectra were recorded on the getter using the Horiba Jobin Yvon LabRAM Aramis Raman spectrometer with a HeCd 325 nm laser in microscope mode with a magnification of 40X.

XPS Spectra. A series of XPS analyses were made on indium foil witness plates and solid KOH-KCl samples using a Scienta 300 XPS Spectrometer or a Kratos Analytical Axis Ultra. The fixed analyzer transmission mode and the sweep acquisition mode were used. The step energy in the survey scan was $0.5\ eV$, and the step energy in the high-resolution scan was

$0.15\ eV$. In the survey scan, the time per step was 0.4 seconds, and the number of sweeps was 4. $C\ 1s$ at $284.5\ eV$ was used as the internal standard.

Using a Scienta 300 XPS spectrometer, XPS was performed at Lehigh University on the indium metal foil witness plate that was initially analyzed by Raman spectroscopy and showed a strong 1982 cm^{-1} IRE peak (Sec, III.C). The sample described supra comprised the In foil exposed to the gases from the ignition of the solid fuel comprising 100 mg Cu + 30 mg deionized water sealed in the aluminum DSC pan.

Additionally, XPS was performed on a KOH:KCl (1:1 wt%) getter placed in a stainless steel tray that was exposed to product gases from three ignitions of the solid fuel 70 mg Ti + 30 mg H_2O sealed in the aluminum DSC pan. For each sequential exposure, the solid fuel maintained under argon was ignited in a sealed primary chamber, and ten seconds after the ignition, the product gas was allowed to flow into a secondary initially sealed chamber containing the KOH:KCl (1:1 wt%) getter that was also under argon.

The ignition product of the solid fuel comprising an explosive was investigated for the presence of hydrino as a product. XPS spectra were also recorded on internal KOH-KCl (1:1 wt%) getter exposed to gases from argon-atmospheric ignition of the solid fuel 50 mg NH_4NO_3 + KOH + KCl (2:1:1 wt.) + 15 mg H_2O sealed in the aluminum DSC pan.

III. Results and Discussion

A. Ignition of H_2O-Based Solid Fuels with a Low Voltage, High Current and Plasma Duration Determination

The control metal foil samples shown in Table 1 as well as a 0.010" diameter gold wire loop were loaded into the electrodes of the Acme 75 KVA welder that was activated to apply high current through each sample. Only resistive heating was observed for the metal foil and wire controls. Additional H_2O-based reaction mixtures that were not catalytic to form hydrinos and served as controls such as 185 mg In + 30 mg $CaCl_2$ + 15 mg H_2O, 185 mg In + 30 mg $ZnCl_2$ + 15 mg H_2O, 185 mg Bi + 30 mg $ZnCl_2$ + 5 mg H_2O, and 185 mg Sn + 30 mg $ZnCl_2$ + 5 mg H_2O showed just resistive heating behavior as well. In contrast, all of the H_2O-based solid fuels underwent a detonation event with a loud blast, brilliant white light emission, and a pressure shock wave. The white light was characteristic of the blackbody emission temperature of about 5000 K confirmed spectroscopically [6]. The sample appeared to have been completely vaporized and atomized to form an ionized, expanding plasma as evidenced by high-speed video using a Phantom v7.3 camera at 6500 frames per second (Figure 2). The plasma was confirmed to be essentially 100% ionized by measuring the Stark broadening of the H Balmer α line [6].

The photodiode-measured temporal duration of the blast event of exemplary solid fuel 100 mg Cu + 30 mg H_2O sealed in the DSC pan was 0.7 ms (Figure 3).

In addition to HOH, $m\ H$ atom catalyst was found to be effective by demonstrating a brilliant light-emitting plasma and blast during the ignition of hydrocarbon-based solid fuel paraffin wax in the DSC pan. As in the case of the H_2O-based solid fuels, blackbody radiation with a temperature of about 5000 K was observed also matching the solar spectrum [6]. Using the fast photodiode, the ignition event was determined to be comprised of two distinct light-emissions-the first had duration of about 500 μs, and the duration of the second was about 750 μs.

Figure 2. Brilliant-light emitting expanding plasma formed from the high-current detonation of the solid fuel Cu + CuO + H_2O filmed at 6500 frames per second.

Figure 3. The temporal full width half maximum light intensity of the ignition event of solid fuel Cu + H_2O measured with a fast photodiode was 0.7 ms.

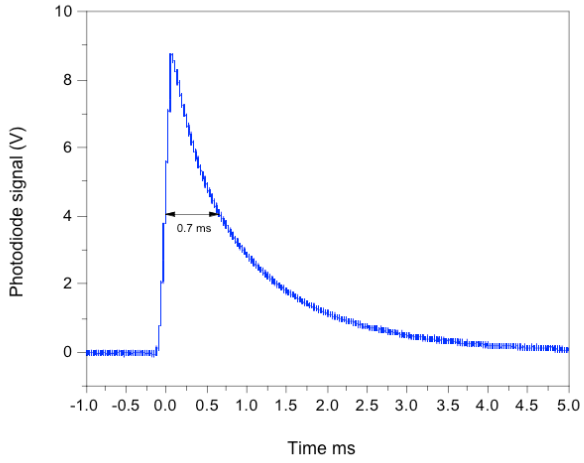

B. Calorimetry of Solid Fuel of the SF-CIHT Cell

Using the metal foils in Table 1, the heat capacity of the calorimeter and electrode apparatus used to measure the energy balance of solid fuel samples was determined to be 8017 J/°C. The calorimetry method used to determine the thermal output from the temperature versus time response following equilibration and ignition was the analytical method described in the operating manual of the Parr 1341 bomb calorimeter [32]. The net energy is the difference between the thermal output and energy input. The gain is the ratio of the thermal energy and the energy input.

Table 1. Determination of the energy balance of solid fuels by bomb calorimetry.

Sample Description[a]	Energy Input (J)	Thermal Output (J)	Net Energy (J)	Gain (X)
80 mg Ti + 30 mg H2O	244.9	1110.8	866.0	4.5
80 mg Ti + 30 mg H2O	126.7	887.4	760.7	7.0
100 mg Cu + 30 mg H2O	204.9	720.4	515.5	3.5
100 mg Cu + 30 mg H2O	104.4	503.1	398.6	4.8
30 mg H2O	293.4	771.8	478.3	2.6

45 mg Cu + 45 mg CuO + 30 mg H2O	196.0	434.0	238.0	2.2
45 mg Cu + 45 mg CuO + 30 mg H2O	203.4	454.1	250.7	2.2
370 mg Ti + 57 mg MgCl2·6H2O, 13mm pellet	427.7	802.6	374.9	1.9
75 mg Ti + 12 mg ZnCl2 + 12 mg H2O, in Cu cap	259.9	787.0	527.1	3.0
148 mg Ag + 52 mg MgCl2·6H2O, 6mm pellet	237.9	505.6	267.6	2.1
148 mg Ag + 52 mg MgCl2·6H2O, 13mm pellet	191.8	501.8	310.0	2.6
30 mg Paraffin Wax	179.6	453.6	274.0	2.5
30 mg Paraffin Wax	194.7	324.8	130.1	1.7
13 mg Nujol Oil	266.8	534.4	267.6	2.0
30 mg Synthetic Oil 10W40	191.3	312.8	121.5	1.6
159 mg Ag + 34 mg NH4NO3 + 7 mg H2O, 6mm pellet	239.3	609.6	370.3	2.5
5 mg NH4NO3 + 1 mg H2O + 10 mg Al	279.8	722.5	442.7	2.6
5 mg NH4NO3	238.7	425.8	187.1	1.8
Setaram Aluminum Pan Control	255.5	262.2	6.8	1.03
0.040” Tungsten Foil Resistive Control	366.6	332.5	-34.1	0.91
0.040” Tungsten Foil Resistive Control	373.9	398.9	25.0	1.07
0.040” Tungsten Foil Resistive Control	1055.0	1069.6	14.6	1.01
0.040” Tungsten Foil Resistive Control	1086.0	1079.9	-6.1	0.99

[a] Samples were sealed in the DSC pan except for pellet and foil samples.

As shown in Table 1, zero net energy balance was consistently measured on the control metal foils as well as the Al DSC pan. In contrast, very significant energy gains as high as 7X were observed for the H_2O-based solid fuel wherein HOH served as catalyst according to Eqs. (5-8). These values are very conservative in that the majority of the input energy was dissipated in the six joints of the calorimeter fuel ignition circuit with only about 20% of the input energy actually delivered to the fuel sample to cause it to ignite. The hierarchy of power production was Ti + H_2O (DSC pan) > Ti + $ZnCl_2$ + H_2O (Cu cap) > Cu + H_2O (DSC pan) > H_2O (DSC pan) > NH_4NO_3 + H_2O + Al > Ti + $MgCl_2 \cdot 6H_2O$ > Ag + $MgCl_2$ + H_2O > Cu + CuO + H_2O (DSC pan) > NH_4NO_3. Additionally, H-based solid fuels comprising oil or wax made some excess energy

wherein nH served as the catalyst according to Eqs. (1-4). The H-based fuels have no theoretical energy since the reactions were run under an argon atmosphere.

The possibility that H_2O may react exothermically with the Al of the DSC pan must be considered in cases where it was used to seal the solid fuel mixture. Consider the solid fuel Cu + H_2O (DSC pan). As shown in Table 2, the reaction of Cu with water is highly endothermic. Specifically, the reaction Cu + H_2O to CuO + H_2 has a positive enthalpy of +130 kJ/mole. Then, the only theoretical energy for conventional chemistry is the reaction of Al with water to form Al_2O_3. This reaction is known to have very slow kinetics. Production of H_2 gas from the Al-water reaction is difficult kinetically; consequently, other approaches such as H_2O plasma are utilized to increase the rate. Even during the detonation of an explosive containing Al, the H_2O oxidation of Al is a slow reaction [33]. Since the ignition of the H_2O-based solid fuel has a duration of less than 1 ms for an inherently slow rate, very little Al_2O_3 would be expected to be formed. This is confirmed by XRD. The compositional analysis results of the XRD of the solid fuel product of a sample of 100 mg Cu mixed with 30 mg of deionized water sealed in a 75 mg Al DSC pan tested in an Ar atmosphere is shown in Table 3. No aluminum oxidation products were observed, thereby demonstrating that none of the output energy recorded by calorimetry is due to Al oxidation. Similarly, XRD on the product of solid fuel Ti + H_2O showed no oxidation of Ti. Thus, the energy released for Cu and Ti, H_2O-based solid fuels was assigned to forming hydrinos. The identification of the hydrino product by multiple methods is given in Sec. IIIC.

Table 2. Thermodynamic parameters of the reaction of Cu metal with H_2O at 298 K [34].

				T(K) =	298
	Cu + H2O(l) to CuO + H2				
	Cu	O2	CuO	H2O	H2
Stoichiometry	1	0	1	1	1
HoF @ 298 K (kJ/mol)	0.000	0.000	-156.059	-285.829	0.000
Δ S @ 298 K (J/molK)	33.162	205.146	42.589	69.948	130.679
Δ H	0.000	0.000	-156.059	-285.829	0.000
Δ G	-9.882	0.000	-168.751	-306.674	-38.942
Δ Hrxn (kJ/mol)	129.770				
Δ Grxn (kJ/mol)	108.863				
n	2				
E°(K) = ~	-0.564 Volts				

Table 3. Results of the XRD of the product of the ignition of the solid fuel 100 mg Cu + 30 mg of deionized water. The ignition was performed in an Ar atmosphere at copper electrodes. No Al_2O_3 was detected; thus, Al oxidation does not contribute to the energy balance.

Cu	20.4 ± 0.2 (>1,000 Å)
$CuAl_2$	24.6 ± 0.4 (958 Å)
$Cu_{31.3}Al_{18.20}$	15.1 ± 0.3 (578 Å)
Cu_4Al	2.1 ± 0.2 (>1,000 Å)
CuAl	0.7 ± 0.1 (613 Å)
$Cu_{0.84}Al_{0.16}$	6.7 ± 0.3 (355 Å)
$Cu_{5.75}Al_{4.5}$	4.5 ± 0.2 (>1,000 Å)
Al	23.6 ± 0.4 (475 Å)
Cu_2O	2.3 ± 0.2 (605 Å)

A major portion of the input energy to ignite the solid fuels in Table 1 was attributed to the melting on the Al DSC pan that is not necessary. For example, a 1 cm^2 nickel screen conductor coated with a thin (<1 mm thick) tape cast coating of NiOOH, 11 wt % carbon, and 27 wt% Ni powder was detonated with a 5 J input energy. This solid fuel produced an extraordinary

amount of EUV continuum energy yield as measured by EUV spectroscopy [6]. Yet, NiOOH solid fuel is more difficult to regenerate in a continuous power cycle compared to M + H_2O (M = Ti, Cu, Al) that only require adding back the H_2O. Rather than use an Al pan, simple pressed metal powders such as Ag + $MgCl_2 \cdot 6H_2O$ that are regenerated by rehydration were tested. These too produced significant excess energy as shown in Table 1. Moreover, there is no theoretical energy from conventional chemistry, the reaction of Ag metal with $MgCl_2 \cdot 6H_2O$, as shown in Table 4. The results of the XRD of the initial solid fuel and the product following the ignition are shown in Tables 5 and 6, respectively. No net positive energy contribution from conventional chemistry can be attributed to the reaction products. A similar analysis for the reactants Ti + $ZnCl_2$ + H_2O shows negligible energy from conventional chemistry.

Table 4. Thermodynamic parameters of the reaction of Ag metal with $MgCl_2 \cdot 6H_2O$ at 298 K [34-36].

				T(K) =	298	
	2Ag + MgCl2.6H2O >> 2AgCl + MgO + H2 + 5H2O					
	Ag	MgCl2.6H2O	H2O	AgCl	MgO	H2
Stoichiometry	2	1	5	2	1	1
HoF @ 298 K (kJ/mol)	0	-2499.01952	-285.829	-127.068	-601.701	0
Δ S @ 298 K (J/molK)	42.677	366.1	69.948	96.232	26.941	130.679
Δ H	0	-2499.01952	-1429.15	-254.136	-601.701	0
Δ G	-25.4355	-2608.11732	-1533.37	-311.49	-609.729	-38.9423
Δ Hrxn (kJ/mol)	214.0375					
Δ Grxn (kJ/mol)	140.0233					
n	2					
E°(K) = ~	-0.7256 Volts					

Table 5. Results of the XRD of the initial solid fuel powder pellet 150 mg Ag + 50 mg $MgCl_2 \cdot 6H_2O$.

$MgCl_2(H_2O)_6$	67.5% (>1,000 Å)
Ag	31.4% (322 Å)
$MgCl_2$	1.1% (>1,000 Å)

Table 6. The XRD results of the solid fuel ignition product of a sample of 150 mg Ag + 50 mg $MgCl_2 \cdot 6H_2O$ tested in an Ar atmosphere showing expected conventional chemistry products that do not contribute positively to the net energy balance.

$MgCl_2(H_2O)_6$	50.9% (>1,000 Å)
Ag	37.2% (336 Å)
Cu	11.4% (>1,000 Å)
AgCl	0.5% (>1,000 Å)

The solid fuel NH_4NO_3 is a well-known energetic material that does release energy upon thermal decomposition. The decomposition reaction of NH_4NO_3 to N_2O and H_2O calculated from the heats of formation [36-38] is exothermic by $\Delta H = -124.4\ kJ / mole\ NH_4NO_3$:

$$NH_4NO_3 \rightarrow N_2O + 2H_2O \tag{9}$$

At elevated temperature, further decomposition occurs. The decomposition reaction energy of NH_4NO_3 to N_2, O_2, and H_2O calculated from the heats of formation [36-38] is exothermic by $\Delta H = -206\ kJ / mole\ NH_4NO_3$:

$$NH_4NO_3 \rightarrow N_2 + 1/2O_2 + 2H_2O \tag{10}$$

For 5 mg NH_4NO_3, the theoretical energy release is 12.8 J (Eq. (10)). Assuming slow kinetics for the oxidation of the Al metal pan [33], the experimental energy balance given in Table 1 is 442.7 J, 34.6 times the most exothermic conventional chemistry reaction given by Eq. (10). The additional energy is attributed to the formation of hydrinos. The high excessive energy balance was confirmed by replacing the conductive Al matrix with non-reactive Ag. The solid fuel 159 mg Ag + 34 mg NH_4NO_3 + 7 mg H_2O, 6 mm pellet produced 370.3 J of net energy, 4.2 times the 88 J (Eq. (10)) maximum theoretical energy by conventional chemistry. The product $H_2(1/4)$ was observed spectroscopically as given in Sec. IIIC. The extraordinary energy and hydrino product identification is very strong evidence that the mechanism of shock wave production in high explosives comprising a source of H and HOH such as those having the elemental

composition CHNO is based on the extraordinary energy released by the formation of $H_2(1/4)$. This result has ramifications for an approach to exploiting the hydrino mechanism of the shock wave of energetic materials to enhance this property as discussed in Sec. IIIC. As given in Sec. IIIA, all of the H_2O-based solid fuels ignited and produced a shock wave behaving as energetic materials with the exception that essentially all the power was in the form of visible radiation rather than pressure-volume [6]. The powers and power densities were extraordinary.

The power and power density of the solid fuels can be determined from the energy released by the reaction given in Table 1, the duration of the release, and the volume of the fuel. Consider the 866.0 J from 80 mg Ti + 30 mg H_2O with a typical duration 0.7 ms as shown in Figure 3. Then, the power is 1.24 MW. Given the fuel volume of 30 μl, the corresponding power density is 41 GW/l. It was observed that the length of the duration of the power generation based on the half-width of the light emission peak could be varied in the range of 2 ms to 100 μs by adjusting the pressure applied to the solid fuel sample by the confining electrodes, the nature of the solid fuel composition, and the waveform of the high current flow through the solid fuel. Thus, the power and power density may be controlled in the range of 0.433 MW to 8.66 MW and 14.4 GW/l to 289 GW/l, respectively.

In addition to HOH, $m\ H$ atom catalyst was tested as evidenced by the observation of thermal energy from a solid fuel comprising a highly conductive material and a source of hydrogen such as a hydrocarbon as shown in Table 1. Since calorimetry was run under an argon atmosphere, no conventional exothermic chemistry was possible. The energy release of over 100 J was significant and confirmatory of $m\ H$ serving as a catalyst to form hydrinos. Moreover, ignition of a hydrocarbon-based solid fuel may produce some matching conditions as those that exist on the surface of the Sun and stars such as white dwarf stars, essentially liquid density of H atoms of a blackbody radiator at 5500-6000 K. So, the kinetics of hydrino formation should be appreciable with the high densities of H formed in the ignition plasma with the presence of the arc current condition. The effectiveness of the $m\ H$ atom catalyst to form hydrinos under the solid fuel ignition plasma conditions was confirmed by the observation of EUV radiation and 5500-6000K blackbody radiation from the ignition of hydrocarbon-based solid fuels [6].

C. Spectroscopic Identification of Molecular Hydrino.

The predicted hydrino product $H_2(1/4)$ was identified by Raman spectroscopy and XPS. Using a Thermo Scientific DXR SmartRaman with a 780 nm diode laser, an absorption peak at 1982 cm^{-1} having a width of 40 cm^{-1} was observed (Figure 4) on the indium metal foil that was exposed to the product gas following the ignition of a series of 50 ignitions of solid fuel pellets. Each pellet comprised 100 mg Cu + 30 mg deionized water sealed in the DSC pan. The only possible elements to consider as the source were In and O. Permutations of controls did not

reproduce the peak, only samples exposed to the gas showed the absorption peak. Since no other element or compound is known that can absorb a single 40 cm^{-1} (0.005 eV) near infrared line at 1.33 eV (the energy of the 780 nm laser minus 2000 cm^{-1}) $H_2(1/4)$ was considered. The absorption peak starting at 1950 cm^{-1} matched the free space rotational energy of $H_2(1/4)$ (0.2414 eV) to four significant figures, and the width of 40 cm^{-1} matches the orbital-nuclear coupling energy splitting [1]. The absorption was assigned to an inverse Raman effect (IRE) [39] peak for the $H_2(1/4)$ rotational energy for the $J' = 1$ to $J'' = 0$ transition [1] as described previously [2-5].

Figure 4. The Raman spectrum obtained on a In metal foil exposed to the product gas from a series of solid fuel ignitions under argon, each comprising 100 mg of Cu mixed with 30 mg of deionized water. Using the Thermo Scientific DXR SmartRaman spectrometer and the 780 nm laser, the spectrum showed an inverse Raman effect peak at 1982 cm^{-1} that matches the free rotor energy of $H_2(1/4)$ (0.2414 eV) to four significant figures.

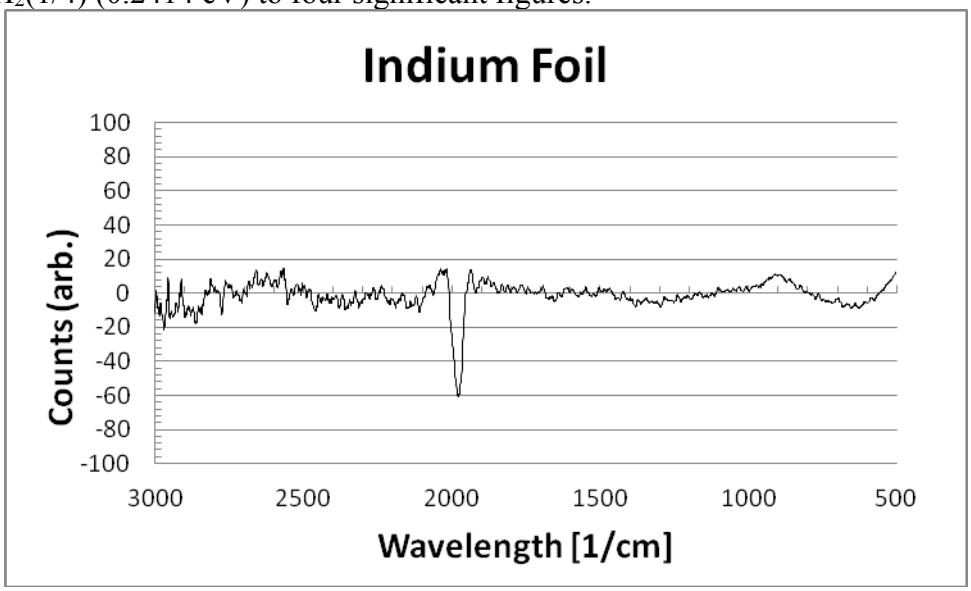

It was reported previously that the ro-vibrational emission (so called 260 nm band) of $H_2(1/4)$ trapped in the crystalline lattice of KCl getters was excited by an incident 6 keV electron beam, and the excitation emission spectrum was recorded by windowless UV spectroscopy on the KCl getter from a sealed reactor of the gun powder reaction, KNO_3 with softwood charcoal having the formulation C_7H_4O. The UV spectrum showed the 260 nm band comprising the peaks Q(0), R(0), R(1), R(2), P(1), P(2), P(3), and P(4) of $H_2(1/4)$ at an integer spacing of p^2 that of H_2, ($p^2 0.01509\ eV$ = 0.249 eV with p = 4) [2]. The hydrino reaction produces 200 times the energy of the conventional chemistry of high explosives that have CHNO

structures favorable for forming HOH and H (Eqs. (5-8)), and the production of hydrino $H_2(1/4)$ by the energetic material gun powder was observed. Therefore, it is reasonable to investigate whether the hydrino reaction is the mechanism for the unique formation of a shock wave by energetic materials. Certain characteristic and identifying signatures would be expected. An extraordinary power and energy balance is predicted by applying a high current to an energetic material since this mechanism increased the kinetics of the hydrino reaction of solid fuels. As shown in Table 1, NH_4NO_3 produced multiples of the possible thermal energy under high-current ignition; wherein ignition uncharacteristically occurred with minute quantities (5 mg) and without a detonator. Hydrino products of this energetic material where sought. The Raman spectra obtained on the In metal foil exposed to the argon-atmosphere ignition of 50 mg of NH_4NO_3 sealed in the DSC pan was recorded using the Thermo Scientific DXR SmartRaman spectrometer and the 780 nm laser. An inverse Raman effect absorption peak was observed at 1988 cm^{-1} (Figure 5) that matches the free rotor energy of $H_2(1/4)$ (0.2414 eV) to four significant figures. Overwhelming evidence is the observation of soft X-ray emission from the NH_4NO_3 ignition. Indeed, 125 J of soft X-ray energy was emitted from 5 mg of NH_4NO_3 ignited in a vacuum chamber and allowed to expand such that the resulting plasma was optically thin for such emission [6]. This energy component exceeds the maximum theoretical from the direct conventional NH_4NO_3 reaction of 12.8 J (Eq. (10)) by a factor of 10. Thus, the dominant source of energy release from this energetic material under these conditions is the formation of $H_2(1/4)$. The implications are that the distinguishing aspect of high explosives that gives rise to a shock wave is not extraordinary conventional chemistry kinetics; rather it is the 200 times higher energy release in the formation of hydrinos. Since H has less than 10 times the mass of CHNO compositions, 2000 times more energy per mass with more effective shock wave yield is feasible with optimization of the hydrino mechanism.

Figure 5. The Raman spectrum recorded on the In metal foil exposed to the product gas from the argon-atmosphere ignition of 50 mg of NH_4NO_3 sealed in the DSC pan. Using the Thermo Scientific DXR SmartRaman spectrometer and the 780 nm laser the spectrum showed the $H_2(1/4)$ inverse Raman effect peak at 1988 cm^{-1}.

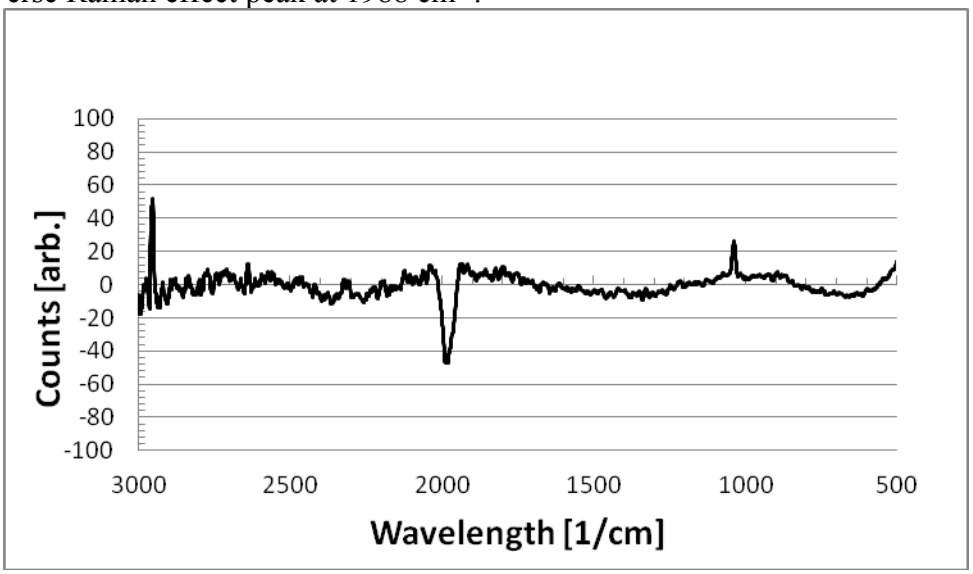

Another successful cross-confirmatory technique in the search for hydrino spectra involved the use of the Raman spectrometer to record the ro-vibration of $H_2(1/4)$ as second order fluorescence matching the previously observed first order spectrum in the ultraviolet, the 260 nm e-beam band [2]. The Raman spectrum of the KOH:KCl (1:1 wt%) getter of the product gas from 50 sequential argon-atmosphere ignitions of solid fuel pellets, each comprising 100 mg Cu + 30 mg deionized water sealed the DSC pan, was recorded using the Horiba Jobin Yvon LabRAM Aramis Raman spectrometer with a HeCd 325 nm laser in microscope mode with a magnification of 40X. No features were observed in the starting material getter. Heating the getter which comprised a hydroxide-halide solid fuel [5] resulted in a low intensity series of 1000 cm^{-1} (0.1234 eV) equal-energy spaced Raman peaks observed in the 8000 cm^{-1} to 18,000 cm^{-1} region. An intense, over an order of magnitude, increase in the series of peaks was observed upon exposure to the ignition product gas. The conversion of the Raman spectrum into the fluorescence or photoluminescence spectrum revealed a match as the second order ro-vibrational spectrum of $H_2(1/4)$ corresponding to the 260 nm band first observed by e-beam excitation [2]. Assigning Q(0) to the most intense peak, the peak assignments given in Table 7 to the Q, R, and P branches for the spectra shown in Figure (6) are Q(0), R(0), R(1), R(2), R(3), R(4), P(1), P(2), P(3), P(4), and P(5) observed at 13,183, 12,199, 11,207, 10,191, 9141, 8100, 14,168, 15,121, 16,064, 16,993, and 17,892 cm^{-1}, respectively. The theoretical transition energies with peak assignments compared with the observed Raman spectrum are shown in

Table 7 and Figure 7. Additional solid fuels 80 mg Ti + 30 mg H_2O and 100 mg Ti + 50 mg Al + 30 mg $ZnCl_2$ + 15 mg H_2O were tested as powders with hydrino getter KOH:KCl (1:1 wt%) that was not heated. The unheated KOH:KCl (1:1 wt%) control did not show the $H_2(1/4)$ ro-vibrational series of peaks, but the solid fuels Ti + H_2O and Ti + Al + $ZnCl_2$ + H_2O showed the same spectral feature as shown in Figures 6 and 7 with the intensity greater for the latter fuel powder.

Table 7. Comparison of the theoretical transition energies and transition assignments [1] with the observed Raman peaks.

Assignment	Calculated (cm^{-1})	Experimental (cm^{-1})	Difference (%)
P(5)	18,055	17,892	0.91
P(4)	17,081	16,993	0.52
P(3)	16,107	16,064	0.27
P(2)	15,134	15,121	0.08
P(1)	14,160	14,168	-0.06
Q(0)	13,186	13,183	0.02
R(0)	12,212	12,199	0.11
R(1)	11,239	11,207	0.28
R(2)	10,265	10,191	0.73
R(3)	9,291	9,141	1.65
R(4)	8,318	8,100	2.69

Figure 6. Raman-mode second-order photoluminescence spectrum of the KOH-KCl (1:1 wt%) getter exposed to the product gases of the ignition of solid fuel samples of 100 mg Cu with 30 mg deionized water sealed in the DSC pan using a Horiba Jobin Yvon LabRam ARAMIS 325nm laser with a 1200 grating over a range of 8000-19,000 cm^{-1} Raman shift.

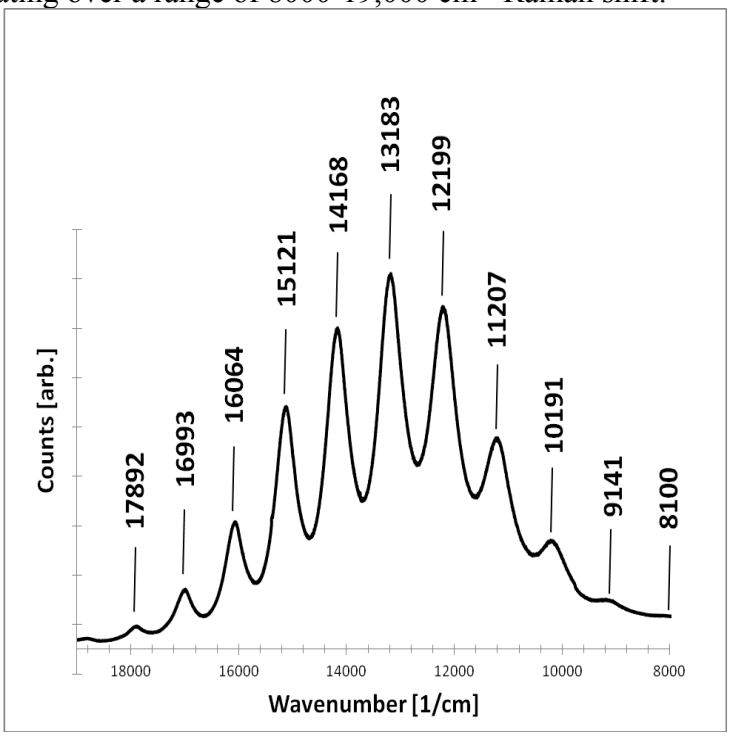

The excitation was deemed to be by the high-energy UV and EUV He and Cd emission of the laser wherein the laser optics are transparent to at least 170 nm and the grating (Labram Aramis 2400g/mm 460mm focal length system with 1024 X 26 μm^2 pixels CCD) is dispersive and has its maximum efficiency at the shorter wavelength side of the spectral range, the same range as the 260 nm band. For example, cadmium has a very intense line at 214.4 nm (5.8 eV) that matches the ro-vibrational excitation energy of $H_2(1/4)$ in KCl matrix based on the e-beam excitation data [2]. The CCD is also most responsive at 500 nm, the region of the second order of the 260 nm band centered at 520 nm.

Overall, the Raman results such as the observation of the 0.241 eV (1940 cm^{-1}) Raman inverse Raman effect peak and the 0.2414 eV-spaced Raman photoluminescence band that matched the 260 nm e-beam spectrum is strong confirmation of molecular hydrino having an internuclear distance that is 1/4 that of H_2. The evidence in the latter case is further substantiated by being in a region having no known first order peaks or possible assignment of matrix peaks at four significant figure agreement with theoretical predictions. Similar results were obtained with

$KCl\text{-}K_3PO_4$ (1:1 wt%) getter. These characteristic ro-vibration signatures of $H_2(1/4)$ match those observed previously on thermal and electrochemical cells [2-5].

Figure 7. A plot comparison between the theoretical energies and assignments given in Table 7 with the observed Raman spectrum.

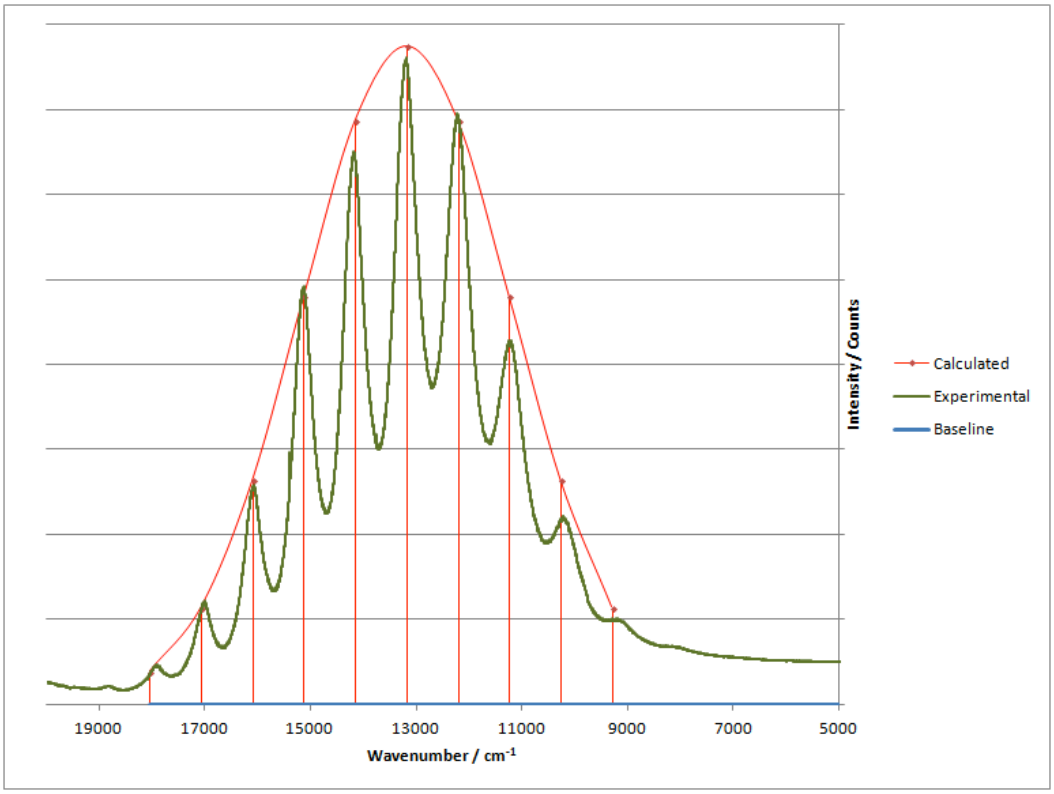

Using a Scienta 300 XPS spectrometer, XPS was performed at Lehigh University on the indium metal foil that showed a strong 1982 cm^{-1} IRE peak following exposure to the gases from the series ignition of the solid fuel pellets, each comprising 100 mg Cu + 30 mg deionized water sealed in the DSC pan. A strong peak was observed at 498.5 eV (Figure 8) that could not be assigned to any known elements. Na, Sn, and Zn being the only possibilities were easy to eliminate based on the absence of any other corresponding peaks of these elements since only In, C, O, and trace K peaks were observed. The peak matched the energy of the theoretically allowed double ionization [2] of molecular hydrino $H_2(1/4)$. This result confirms the molecular hydrino assignment by Raman spectroscopy, the inverse Raman effect absorption peak centered at 1982 cm^{-1}.

Figure 8. XPS spectra recorded on the indium metal foil exposed to gases from sequential argon-atmosphere ignitions of the solid fuel 100 mg Cu + 30 mg deionized water sealed in the

DSC pan. (A) A survey spectrum showing only the elements In, C, O, and trace K peaks were present. (B) High-resolution spectrum showing a peak at 498.5 eV assigned to $H_2(1/4)$ wherein other possibilities were eliminated based on the absence of any other corresponding primary element peaks.

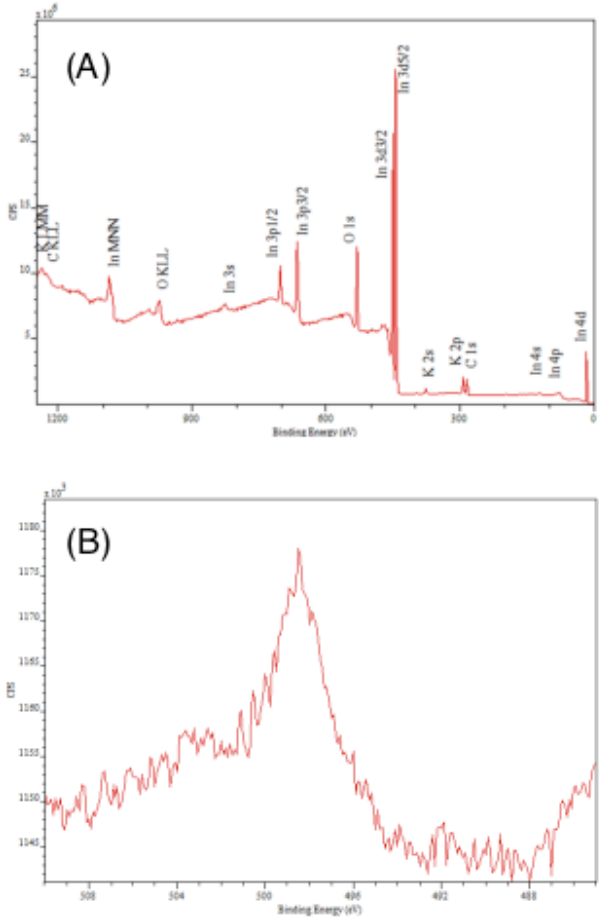

Using the Lehigh University Scienta 300 XPS spectrometer, XPS spectra were also recorded on the KOH-KCl (1:1 wt%) getter sequentially exposed to gases from three ignitions of the solid fuel 70 mg Ti + 30 mg H_2O sealed in the aluminum DSC pan. A strong peak was observed at 496 eV (Figure 9) that was assigned to $H_2(1/4)$ since only K, C, O, N, and trace I peaks were observed. None of these elements have a peak in the region of interest and elements that have a peak in the region of 496 eV were not present based on the absence of any other corresponding primary element peaks.

Figure 9. XPS spectra recorded on KOH-KCl (1:1 wt%) getter exposed to gases from sequential argon-atmosphere ignitions of the solid fuel 85 mg of Ti mixed with 30 mg of deionized water sealed in the DSC pan. (A) A survey spectrum showing only the elements K, C, O, N, and trace I peaks were present. (B) High-resolution spectrum showing a peak at 496 eV assigned to $H_2(1/4)$ wherein other possibilities were eliminated based on the absence of any other corresponding primary element peaks.

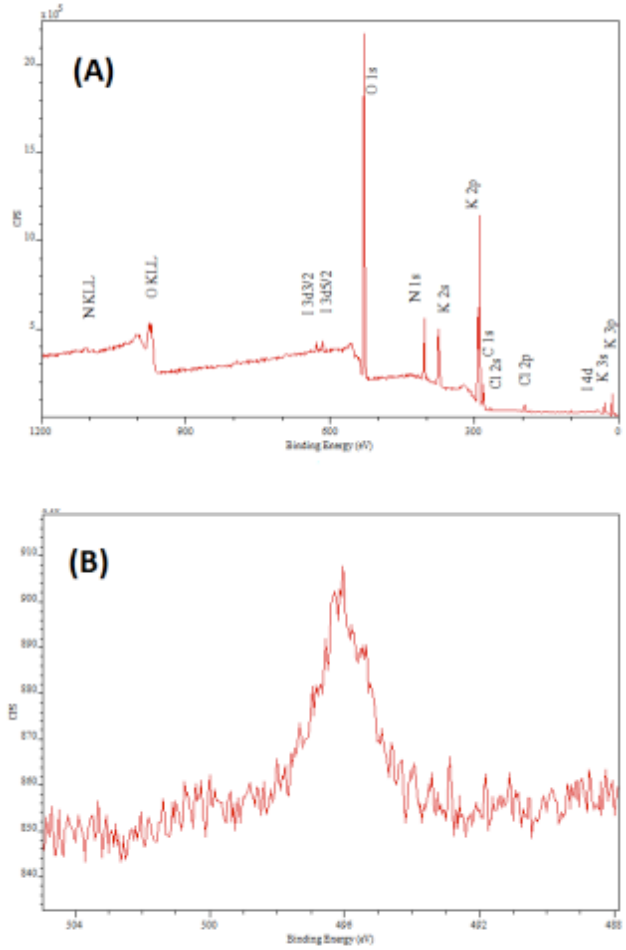

Using the Lehigh University Scienta 300 XPS spectrometer, XPS spectra were also recorded on internal KOH-KCl (1:1 wt%) getter exposed to gases from argon-atmospheric ignition of the solid fuel 50 mg NH_4NO_3 + KOH + KCl (2:1:1 wt.) + 15 mg H_2O sealed in the aluminum DSC pan. A strong peak was observed at 496 eV (Figure 10) that was assigned to $H_2(1/4)$ since only K, Cu, Cl, Si, Al, C, O, and trace F peaks were observed. None of these

elements have a peak in the region of interest and elements that have a peak in the region of 496 eV were not present based on the absence of any other corresponding primary element peaks.

Figure 10. XPS spectra recorded on internal KOH-KCl (1:1 wt%) getter exposed to gases argon-atmospheric ignition of the solid fuel 50 mg NH_4NO_3 + KOH + KCl (2:1:1 wt.) + 15 mg H_2O sealed in the aluminum DSC pan. (A) A survey spectrum showing only the elements K, Cu, Cl, Si, Al, C, O, and trace F peaks were present. (B) High-resolution spectrum showing a peak at 496 eV assigned to $H_2(1/4)$ wherein other possibilities were eliminated based on the absence of any other corresponding primary element peaks.

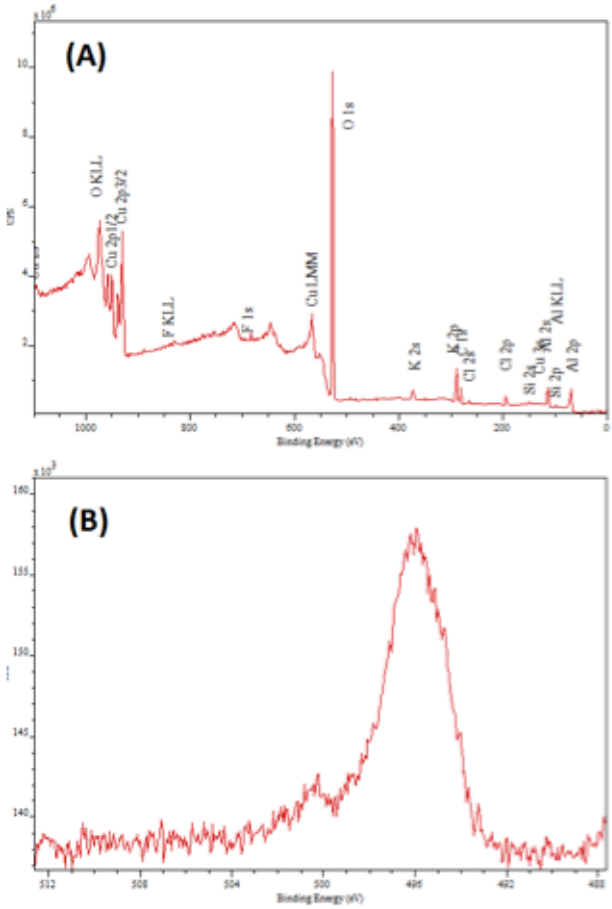

IV. Conclusion

A recent breakthrough is a Solid Fuel-Catalyst-Induced-Hydrino-Transition (SF-CIHT) cell that produces hundreds of thousands of watts of power in a volume that is a few hundred thousandths of a liter corresponding to a power density of tens of billions of watts per liter [4].

Using a water-based solid fuel confined between two electrodes of a SF-CIHT cell incorporated in a bomb calorimeter, and applying a current of 10,000 - 25,000 A through the fuel gave results that confirmed the prior spectroscopic results of power and power density [4]. No chemical reaction could account for the energy released based on conventional thermodynamic predictions and XRD results. Moreover, using multiple spectroscopic techniques, the source of energy was confirmed to be the hydrino $H_2(1/4)$, the predicted product of HOH catalyst. Raman spectroscopy showed an IRE peak at 1982 cm^{-1} that matched the rotational energy of $H_2(1/4)$. Photoluminescence emission spectroscopy showed a series of 1000 cm^{-1} (0.1234 eV) equal-energy spaced Raman peaks observed in the 8000 cm^{-1} to 18,000 cm^{-1} region that matched the ro-vibration transitions of $H_2(1/4)$. And, X-ray photoelectron spectroscopy (XPS) showed a peak at 498.5 eV or 496 eV, depending on the matrix, that matched the predicted total energy of $H_2(1/4)$ wherein other possibilities for the assignment other than $H_2(1/4)$ were eliminated based on the absence of any other corresponding primary element peaks. The SF-CIHT cell is a powerful new source of energy based on the high kinetics of the transition of the hydrogen of H_2O to hydrino in the presence of a high current.

References

1. R. Mills, *The Grand Unified Theory of Classical Physics*; 2014 Edition, posted at http://www.blacklightpower.com/theory-2/book/book-download/.
2. R. Mills, X Yu, Y. Lu, G Chu, J. He, J. Lotoski, "Catalyst induced hydrino transition (CIHT) electrochemical cell," (2012), Int. J. Energy Res., (2013), DOI: 10.1002/er.3142.
3. R. Mills, J. Lotoski, J. Kong, G. Chu, J. He, J. Trevey, "High-Power-Density Catalyst Induced Hydrino Transition (CIHT) Electrochemical Cell." Int. J. Hydrogen Energy, 39 (2014), pp. 14512–14530 DOI: 10.1016/j.ijhydene.2014.06.153.
4. R. Mills, "Power generation systems and methods regarding same", PCT/IB2014/058177.
5. R. Mills, J. Lotoski, W. Good, J. He, "Solid Fuels that Form HOH Catalyst," Int'l J. Hydrogen Energy, 39 (2014), pp. 11930–11944 DOI: 10.1016/j.ijhydene.2014.05.170.
6. R. Mills, Y. Lu, "Mechanism of soft X-ray continuum radiation from low-energy pinch discharges of hydrogen and ultra-low field ignition of solid fuels," submitted.
7. R. L. Mills, R. Booker, Y. Lu, "Soft X-ray Continuum Radiation from Low-Energy Pinch Discharges of Hydrogen," J. Plasma Physics, Vol. 79, (2013), pp 489-507; doi: 10.1017/S0022377812001109.
8. R. L. Mills, Y. Lu, "Hydrino continuum transitions with cutoffs at 22.8 nm and 10.1 nm," Int. J. Hydrogen Energy, 35 (2010), pp. 8446-8456, doi: 10.1016/j.ijhydene.2010.05.098.

9. R. L. Mills, Y. Lu, K. Akhtar, "Spectroscopic observation of helium-ion- and hydrogen-catalyzed hydrino transitions," Cent. Eur. J. Phys., 8 (2010), pp. 318-339, doi: 10.2478/s11534-009-0106-9.
10. R. L. Mills, Y. Lu, "Time-resolved hydrino continuum transitions with cutoffs at 22.8 nm and 10.1 nm," Eur. Phys. J. D, Vol. 64, (2011), pp. 65, DOI: 10.1140/epjd/e2011-20246-5.
11. A. Bykanov, "Validation of the observation of soft X-ray continuum radiation from low energy pinch discharges in the presence of molecular hydrogen," http://www.blacklightpower.com/wp-content/uploads/pdf/GEN3_Harvard.pdf.
12. M. Kuraica, N. Konjevic, "Line shapes of atomic hydrogen in a plane-cathode abnormal glow discharge," Physical Review A, Volume 46, No. 7, October (1992), pp. 4429-4432.
13. M. Kuraica, N. Konjevic, M. Platisa and D. Pantelic, *Spectrochimica Acta* Vol. 47, 1173 (1992).
14. I. R. Videnovic, N. Konjevic, M. M. Kuraica, "Spectroscopic investigations of a cathode fall region of the Grimm-type glow discharge," Spectrochimica Acta, Part B, Vol. 51, (1996), pp. 1707-1731.
15. S. Alexiou, E. Leboucher-Dalimier, "Hydrogen Balmer-α in dense plasmas," Phys. Rev. E, Vol. 60, No. 3, (1999), pp. 3436-3438.
16. S. Djurovic, J. R. Roberts, "Hydrogen Balmer alpha line shapes for hydrogen-argon mixtures in a low-pressure rf discharge," J. Appl. Phys., Vol. 74, No. 11, (1993), pp. 6558-6565.
17. S. B. Radovanov, K. Dzierzega, J. R. Roberts, J. K. Olthoff, "Time-resolved Balmer-alpha emission from fast hydrogen atoms in low pressure, radio-frequency discharges in hydrogen," Appl. Phys. Lett., Vol. 66, No. 20, (1995), pp. 2637-2639.
18. S. B. Radovanov, J. K. Olthoff, R. J. Van Brunt, S. Djurovic, "Ion kinetic-energy distributions and Balmer-alpha (H_α) excitation in $Ar - H_2$ radio-frequency discharges," J. Appl. Phys., Vol. 78, No. 2, (1995), pp. 746-757.
19. G. Baravian, Y. Chouan, A. Ricard, G. Sultan, J. Appl. Phys., Vol. 61, (1987), p. 5249.
20. A. V. Phelps, J. Phys. Chem. Ref. Data, Vol. 21, (1992), p. 883.
21. C. Barbeau, J. Jolly, "Spectroscopic investigation of energetic atoms in a DC hydrogen glow discharge," Journal of Physics, D, Applied Physics, Vol. 23, (1990), pp. 1168-1174.
22. S. A. Bzenic, S. B. Radovanov, S. B. Vrhovac, Z. B. Velikic, and B. M. Jelenkovic, Chem. Phys. Lett., Vol. 184, (1991), pp. 108-112.
23. E. L. Ayers, W. Benesch, "Shapes of atomic-hydrogen lines produced at a cathode surface," Physical Review A, Vol. 37, No. 1, (1988), pp. 194-199.
24. W. Benesch, E. Li, "Line shapes of atomic hydrogen in hollow-cathode discharges," Optic Letters, Vol. 9, No. 8, (1984), pp. 338-340.
25. K. Akhtar, J. Scharer, R. L. Mills, "Substantial Doppler broadening of atomic-hydrogen lines

in DC and capacitively coupled RF plasmas**,"** J. Phys. D, Applied Physics, Vol. 42, (2009), 42 135207 (2009) doi:10.1088/0022-3727/42/13/135207.

26. R. Mills, K. Akhtar, "Tests of features of field-acceleration models for the extraordinary selective H Balmer α broadening in certain hydrogen mixed plasmas," Int. J. Hydrogen Energy, Vol. 34, (2009), pp. 6465-6477.
27. R. L. Mills, B. Dhandapani, K. Akhtar, "Excessive Balmer α line broadening of water-vapor capacitively-coupled RF discharge plasmas," Int. J. Hydrogen Energy, Vol. 33, (2008), pp. 802-815.
28. R. Mills, P. Ray, B. Dhandapani, "Evidence of an energy transfer reaction between atomic hydrogen and argon II or helium II as the source of excessively hot H atoms in RF plasmas," Journal of Plasma Physics, (2006), Vol. 72, Issue 4, pp. 469-484.
29. J. Phillips, C-K Chen, K. Akhtar, B. Dhandapani, R. Mills, "Evidence of catalytic production of hot hydrogen in RF generated hydrogen/argon plasmas," International Journal of Hydrogen Energy, Vol. 32(14), (2007), 3010-3025.
30. R. L. Mills, P. C. Ray, R. M. Mayo, M. Nansteel, B. Dhandapani, J. Phillips, "Spectroscopic study of unique line broadening and inversion in low pressure microwave generated water plasmas," J. Plasma Physics, Vol. 71, Part 6, (2005), pp. 877-888.
31. R. L. Mills, K. Akhtar, "Fast H in hydrogen mixed gas microwave plasmas when an atomic hydrogen supporting surface was present," Int. J. Hydrogen Energy, 35 (2010), pp. 2546-2555, doi:10.1016/j.ijhydene.2009.12.148.
32. http://www.parrinst.com/products/oxygen-bomb-calorimeters/1341-plain-jacket-bomb-calorimeter/.
33. G. F. Kinney, K. J. Graham, *Explosive Shocks in Air*, Second Edition, Springer Science + Business Media, LLC, (1985).
34. http://physics.nist.gov/PhysRefData/Handbook/Tables/cadmiumtable2.htm.
35. http://www.new.chemistry-teaching-resources.com/Resources/ADVH/Documents/Units/ThermoChemistry%20LO's%20and%20Q's.pdf.
36. J. A. Dean, *Lange's Handbook of Chemistry*, Fifteenth Edition, McGraw-Hill Professional, New York, (1999).
37. D. R. Lide, *CRC Handbook of Chemistry and Physics*, 88th Edition, CRC Press, Taylor & Francis, Boca Raton, (2007-8).
38. O. Knacke, O. Kubascheeski, K. Hesselmann, *Thermochemical Properties of Inorganic Substances*, 2nd Ed., Springer-Verlag Berlin, Heidelberg 1991.
39. W. J. Jones, B. P. Stoicheff, "Inverse Raman spectra: Induced absorption at optical frequencies," Physcial Review Letters, Vol. 13, No. 22, (1964), pp. 657-659.